Advanced optical modeling of TiN metal hard mask for scatterometric critical dimension metrology

Peter Ebersbach[a], Adam M. Urbanowicz[b], Dmitriy Likhachev[a], Carsten Hartig[a]

[a] GLOBALFOUNDRIES Dresden Module One LLC & Co. KG, Wilschdorfer Landstr. 101, 01109 Dresden, Germany
[b] Nova Measuring Instruments, Moritzburger Weg 67, 01109 Dresden, Germany

ABSTRACT

The majority of scatterometric production control models assume constant optical properties of the materials and only dimensional parameters are allowed to vary. However, this assumption, especially in case of thin-metal films, negatively impacts model precision and accuracy. In this work we focus on optical modeling of the TiN metal hardmask for scatterometry applications. Since the dielectric function of TiN exhibits thickness dependence, we had to take this fact into account. Moreover, presence of the highly absorbing films influences extracted thicknesses of dielectric layers underneath the metal films. The later phenomenon is often not reflected by goodness of fit. We show that accurate optical modeling of metal is essential to achieve desired scatterometric model quality for automatic process control in microelectronic production. Presented modeling methodology can be applied to other TiN applications such as diffusion barriers and metal gates as well as for other metals used in microelectronic manufacturing for all technology nodes.

Keywords: TiN hardmask, optical properties, thin metals, optical modeling, scatterometry, OCD

1. INTRODUCTION

Titanium nitride (TiN) is widely utilized metal in semiconductor manufacturing. It has a variety of applications such as gate material, metal hard mask and diffusion barrier. Properties of TiN depend on its structure and composition. For instance, stoichiometric crystalline TiN is a good conductor and used as a diffusion barrier material, whereas amorphous or nitrogen deficient TiN is a very good insulator.[1] In this paper we focus on optical properties and their relation to material characteristic of TiN hard mask[2,3] for advanced in-line production control in first metal levels of 22 nm FD SOI technology. A typical optical process control structure is illustrated in Figure 1. Optical dimensions such as the TiN thickness and middle CDs (critical dimensions) as well as ILD (interlayer dielectric) undercut need to be well controlled. We demonstrate that set up of accurate optical model for such stacks is a non-trivial task due to the presence of a highly absorbing film, namely TiN. Optical properties of thin-metal films vary with deposition conditions, surface oxidation/roughness and film thicknesses.[4,5,6] This creates significant challenges for optical critical dimensions (OCD) modeling of the stacks consisting of thin metals. Typically, OCD models assume fixed optical properties of line and background materials. Fixed film optical properties and surface anomalies not included in an optical model will impact the OCD results. Therefore, OCD models need calibration and periodic verification. Typically model results are correlated with reference metrology techniques such as scanning electron microscopy (SEM), atomic force microscopy (AFM) or transmission electron microscopy (TEM). In practice, the assumption of fixed optical properties (constant n&k) of the most critical materials leads to higher model error with shrinking stack dimensions. Reduced error tolerance with advanced technology nodes requires advanced modeling techniques. In this work we focus on accurate optical modeling of TiN metal as well as active parameter isolation (API). On the other hand, an accurate modeling might bring additional information related to important material parameters such as stress or resistance.

Metrology, Inspection, and Process Control for Microlithography XXXI, edited by Martha I. Sanchez, Vladimir A. Ukraintsev
Proc. of SPIE Vol. 10145, 101451G · © 2017 SPIE · CCC code: 0277-786X/17/$18 · doi: 10.1117/12.2258659

Downloaded From: http://proceedings.spiedigitallibrary.org/ on 04/30/2017 Terms of Use: http://spiedigitallibrary.org/ss/termsofuse.aspx

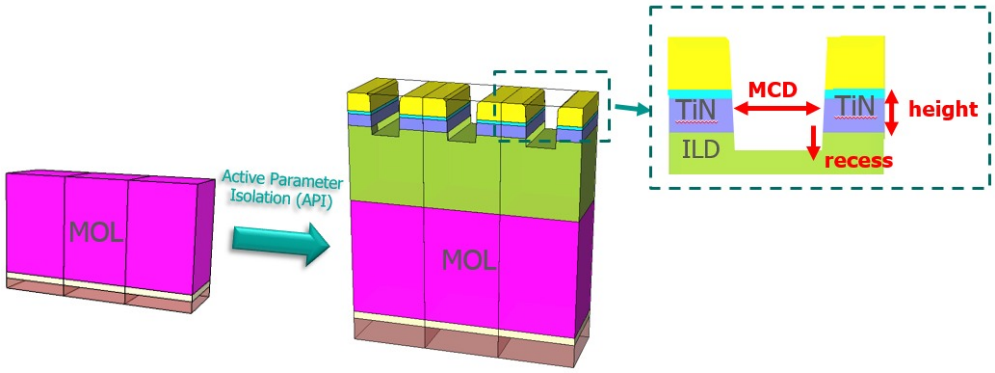

Figure 1: Typical structure to control in 22 nm FDSOI technology in M1 metallization level. Advanced OCD model requires precise TiN modeling. Light blue layer represents TiN roughness layer. In order to break correlations between multi dielectric stack Active Parameter Isolation (API) of the model parameters from previous step might be required.

2. METHODS AND MEASURED STRUCTURES

2.1 Wafers preparation

In order to model optical properties, TiN with various thicknesses has been deposited on blanket 300 mm Si wafers (Figure 2). TiN hard mask (HM) has been deposited by physical vapor deposition process (PVD). Thin oxide was used for interference enhancement.[7] In our analysis we combine the existence of thick (~1000 Å) transparent film (SiO_2) on Si substrate. The oxide was used to apply an interference enhancement approach to enhance the measured information and therefore, determine the TiN optical properties with high accuracy. Despite the used set of blanket wafers for material characterization, product wafers were used as well. We compared four product wafers measured full map with the stack as shown in Figure 1. We used as reference data set inline CD-SEM and AFM data. CD-SEM data were collected on column-exposure matrix (CEM) wafer. DoE used in this paper is depicted in Figure 14 and Figure 15 and discussed in chapter 3.5.

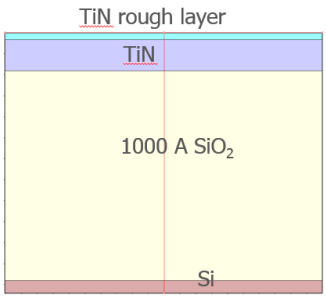

Figure 2: Schematic representation of material stack used for TiN HM material characterization.

2.2 Metrology

We used production-grade spectroscopic reflectometer with a unique multi-channel configuration featuring normal and oblique incidence spectroscopic reflectometry (SR). SR acquires reflection spectra from the sample using several channels of information. In this work two configuration of SR were used for study of blanket wafers. Configuration 2 had an additional optical information channels. For an additional analysis of blanket TiN films research-grade variable-angle spectroscopic ellipsometer (VASE) was used. The measurement spot size of VASE system is significantly larger than for production grade reflectometer. VASE is a powerful technique for multi-layer optical measurements since the

Downloaded From: http://proceedings.spiedigitallibrary.org/ on 04/30/2017 Terms of Use: http://spiedigitallibrary.org/ss/termsofuse.aspx

ellipsometric angles Ψ and Δ are measured as a functions of both wavelength and angle of incidence (AOI). VASE is characterized by higher sensitivity and accuracy than standard SE due to additional optical information provided by the various AOI's. To validate the obtained modeling results for blanket wafers the x-ray reflectivity (XRR) system has been used. The OCD measurements were performed using production grade SR with configuration 1. We modeled all samples using Nova modeling software. Statistical data analysis has been performed using JMP software.

3. RESULTS AND DISCUSSION

At first, we discuss the need for more accurate modeling of the TiN metal layers (chapter 3.1). Next we examine obtained optical properties of the TiN films with two different compositions and a variety of thicknesses (chapter 3.2). In Chapter 3.3 we focus on modeling of the TiN layers with a thickness range used for typical production applications. Furthermore, we propose an additional metric for model correctness in chapter 3.4. And finally in chapter 3.5 we demonstrate an application of an established metal model used in a production grade OCD solution.

3.1 Effect of top metal layer on model with dielectric stack

The presence of a metal layer on top of a dielectric stack results in a more complex optical modeling. A typical structure with metal layer on top is shown in Figure 3. Accurate modeling of the top layer will lead to more accurate results of the thicknesses of dielectrics underneath the TiN layer. To demonstrate that we compare modeled reflectometry data for several wafers with ILD2 thickness split as shown in Figure 4. Here we show the data for ILD1/ILD2 stack (POR) model without the TiN hard mask. The other two models use the same model of ILD1/ILD2 but two different models for TiN. The change of the TiN model (all other dielectric models remain the same) results in variation in DoE split. It is clearly seen that the achieved thickness values and in-wafer thickness variation depend on the TiN optical model. The model with lower merit function values (POR/TiN1) results in thickness values which agree less with the target values than ones obtained from the model with higher merit function values (POR/TiN2). However, we should bear in mind that the selection of the best model should be based not only on goodness of fit but also on parametric complexity of the model.

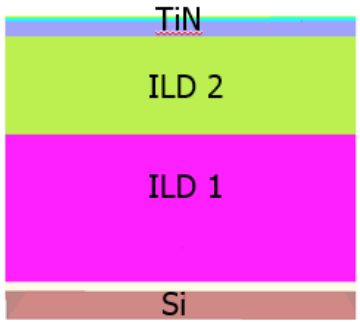

Figure 3: Typical thin film stack with TiN hardmask on top.

Downloaded From: http://proceedings.spiedigitallibrary.org/ on 04/30/2017 Terms of Use: http://spiedigitallibrary.org/ss/termsofuse.aspx

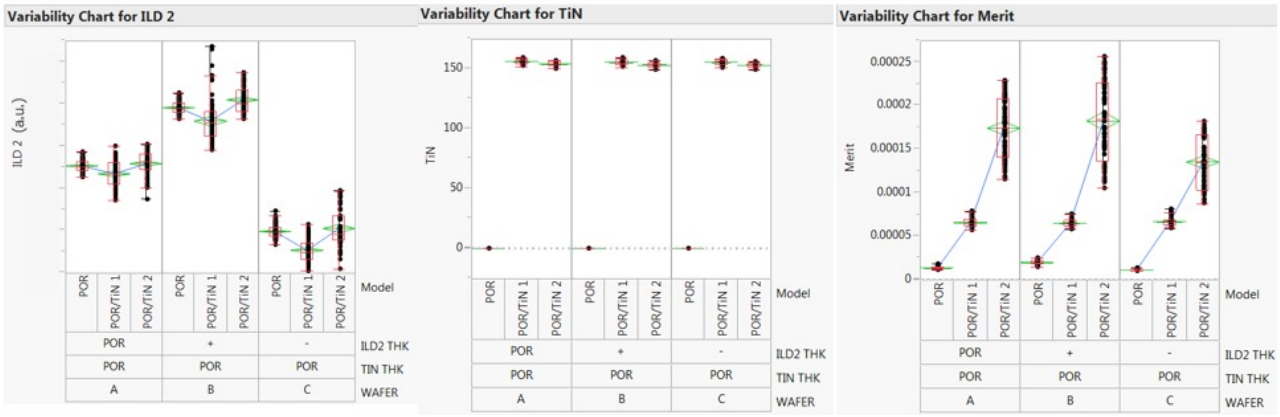

Figure 4: Design of experiment (DoE) scheme for three full map data of three production wafers.

3.2 Dependence of optical properties of TiN on its thickness and composition

Optical properties of a metal film are linked to its structure. The growth of thin films proceeds through consecutive stages characterized by specific processes of structure evolution: nucleation, island growth, coalescence of islands, formation of polycrystalline islands and channels, development of a continuous structure and thickness growth (Figure 5a).[8] The analysis of the structure evolution and that of the effects of the deposition parameters on the structure and on the appearance of peculiar structural features leads to the conclusion that the comprehensive description of the formation of the various structures is possible by selecting the basic structure forming phenomena. For PVD TiN HM deposition process the film structure can be approximately represented using metal deposition zone diagram as shown in Figure 5b.[2] In Zone I it is column film, and in Zone T, the film transforms from column to crystal. The traditional PVD TiN process condition is close to Zone T (a). In this area, the film is denser and the surface mobility is much higher. For HM application the material must be tuned for lower possible stress. This is achieved typically in high pressure area marked c). When the DC power decreases, the wafer surface temperature will decrease, too. So it will cause lower TiN stress as well.

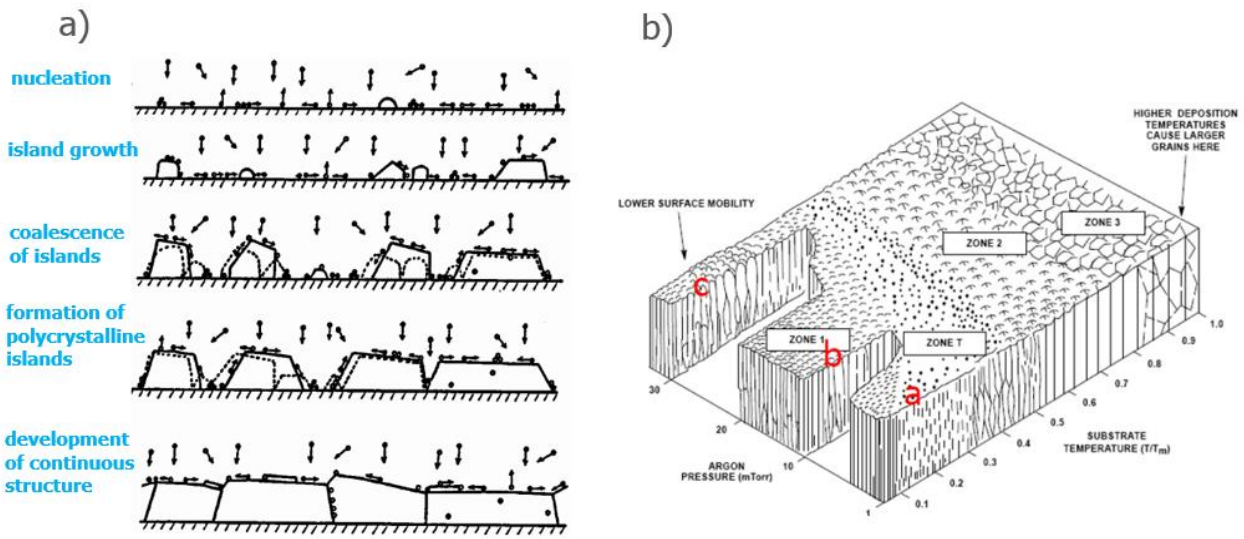

Figure 5: a) Schematic diagram illustrating typical PVD film growth process.[8] b) sketch showing a metal deposition zone diagram typical for PVD TiN HM deposition processes.[2]

Downloaded From: http://proceedings.spiedigitallibrary.org/ on 04/30/2017 Terms of Use: http://spiedigitallibrary.org/ss/termsofuse.aspx

Figure 6 shows the obtained optical properties of the TiN films with lower thicknesses and two different deposition conditions. Multi-oscillator Tauc-Lorentz model was used to fit the data. Thickness dependence of the optical properties (*n*&*k*'s) is clearly visible for both deposition conditions: with low N-content and with high N-content. Furthermore, N-content has influence on TiN properties as well. Apart from thickness and composition dependencies on optical properties, two other factors influence the TiN dispersion: surface oxidation/roughness and variability due to process conditions as also demonstrated in Figure 6. The surface roughness of metal films can be described using effective medium approximation (EMA) and is discussed in Chapter 3.3. Furthermore, extinction coefficient (*k*) clearly increases with thickness especially in red and near-infrared (NIR) parts of the spectra (600-1000 nm). This area is related to Drude absorption. Metallic films show Drude absorption in NIR by conduction electrons. The Drude model describes ideal model of material resistance. Drude resistance can be indirectly link to film resistance. Furthermore, thin metals show significant deviation from bulk optical properties up to 100 Å.[4,5] According to literature[9], the metal films transform into a more granular form (tens of angstrom range) with decreasing thickness, therefore, their behavior deviates from bulk material. The optical conductivity depends on the capacitive coupling of the islands and thus increases with frequency (see the film growth -illustrated in Figure 5a). Below some thickness threshold, called percolation threshold, one can observe the metal-insulator transition (metallic behavior disappears). This results in abrupt decrease in real part of dielectric function due to Drude absorption. Different metals have different percolation threshold, for instance, for titanium it is equal to 25 Å.[5, 10] In practice, the optical properties of TiN need to be linked with specific process conditions, i.e., by using metal deposition zone diagram as shown in Figure 5b.[2]

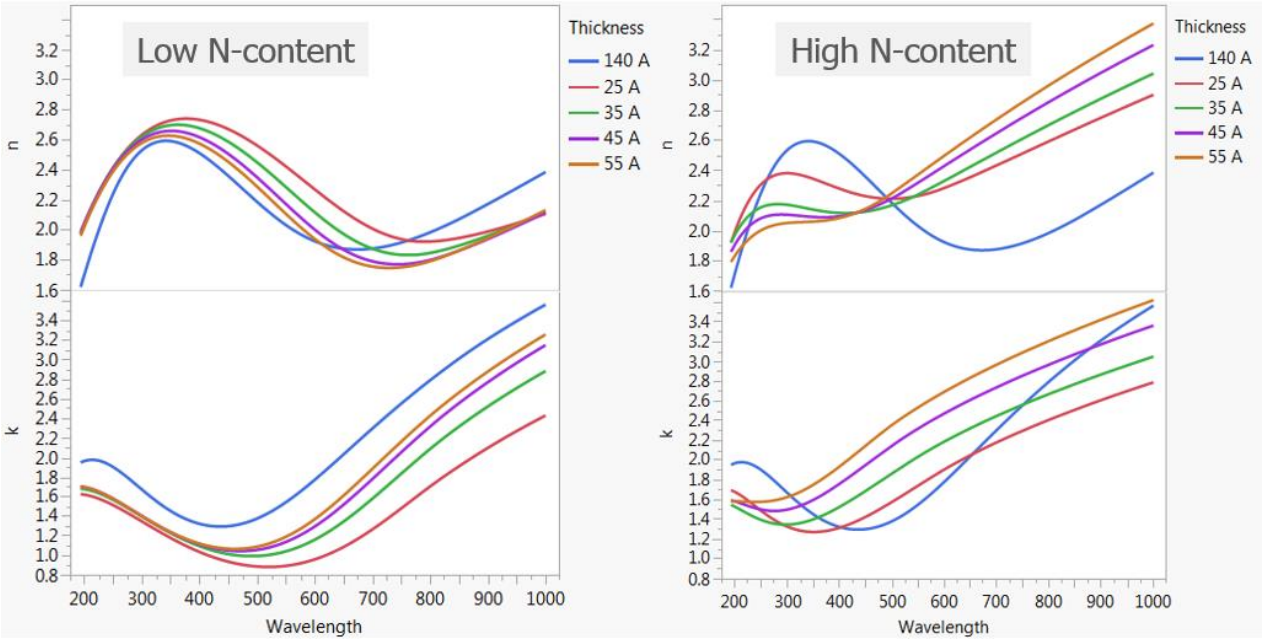

Figure 6: Optical properties of PVD deposited TiN hardmask material with different thicknesses and two compositions.

3.3 Accurate optical modeling of TiN layer

We model optical properties of TiN using the measured data from blanket Si wafers with a stack represented in Figure 2. The model is targeted to describe a broad thickness range. The initial model consists of a multi-oscillator Tauc-Lorentz model. On the top of the stack a roughness layer was also included. The TiN roughness is modeled by an effective-medium-approximation (EMA) layer. [4] The EMA assumes 50% of air fraction in TiN. We consider that as a sufficient approximation for the top layer. There are also other approaches to this layer i.e. treat it as a titanium oxide. Furthermore, during processing (not in our case) some residues can be present due to plasma processing. For instance, the C, F, N, and

Downloaded From: http://proceedings.spiedigitallibrary.org/ on 04/30/2017 Terms of Use: http://spiedigitallibrary.org/ss/termsofuse.aspx

O containing residues might exist and their optical influence can be enhanced due to the exposure to ambient (i.e. after wafer removal from an plasma etch chamber).[11] Furthermore, the TiN deposition on low-*k* dielectric can result in ~10 Å-thick interface which is some cases needs to be included in a production model. The modeled dispersions of TiN with different thicknesses are shown in Figure 7. Literature describes a deviation from bulk optical properties for the thickness up to 100 Å.[4,5] However in the evaluated range of 125-345 Å we still observe thickness dependence that affects model output as shown in Figure 7. The thickness dependence starts to have smaller effect on n&k's for thicknesses above 250 Å. The plots on the right side show refractive index n at 300 nm and extinction coefficient k at 900 nm as function of nominal TiN thickness. Those WLs seem to be most sensitive on the change related to the thickness. Drude resistance should correlate to k at 900 nm. And vice versa this characteristic reflects the TiN material properties. For instance, the material properties effect on TiN HM stress that is one of the fundamental manufacturing problems related to TiN hard mask technology.[12,13,14] Furthermore, the plots in figure 7b justify suitability of the presented dispersion set for an alloy model approach.

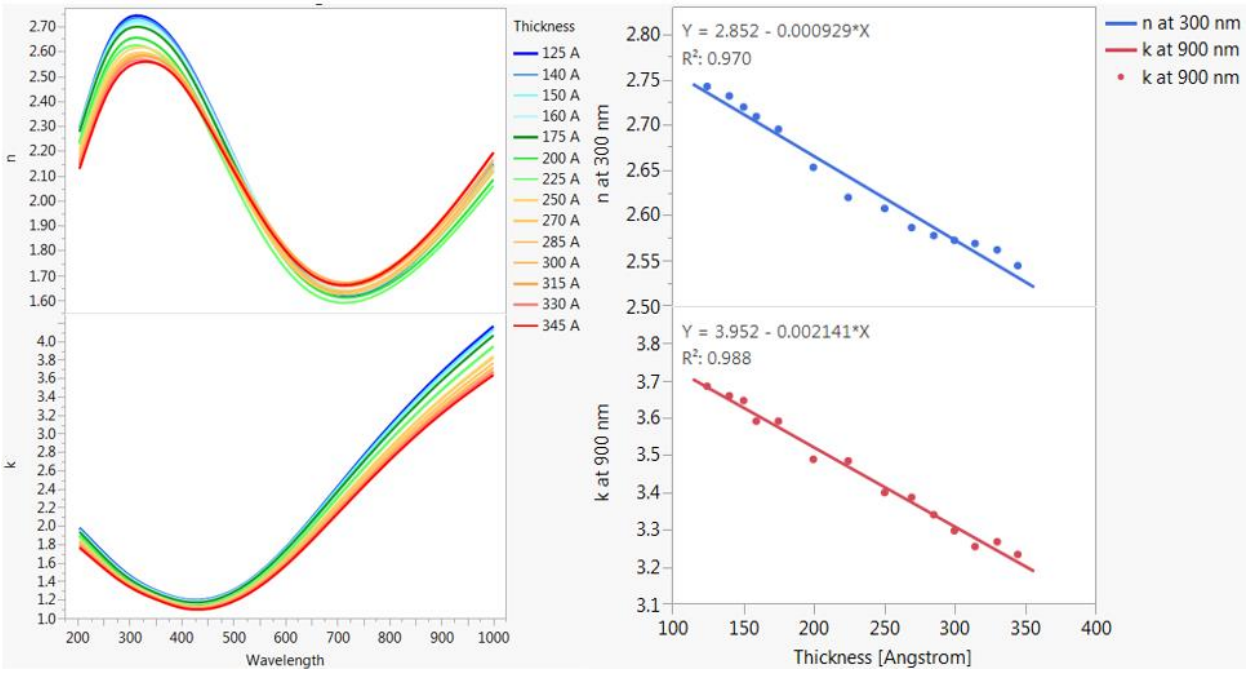

Figure 7: Optical properties of TiN hardmask within thickness range describing process variation. Figure 7a shows the *n*&*k* curves use to build the alloy model. Figure 7b demonstrates linearity of the refractive index *n* at λ = 300 nm and extinction coefficient λ = 900 nm and justifies the use of the alloy model.

In order to prove our model, the optical data for 125-250 Å thickness range were correlated to XRR. We use the optical model for both VASE and multi-channel SR. In all cases a slope close to unity is demonstrated. The R^2 coefficient is the best in case of the VASE data. Since this is a research-grade system with a large spot this is expected. We also tested SR with basic channel configuration (configuration 1) and with the additional channels (configuration 2). The results show that more information channels improve fit to reference data.

Downloaded From: http://proceedings.spiedigitallibrary.org/ on 04/30/2017 Terms of Use: http://spiedigitallibrary.org/ss/termsofuse.aspx

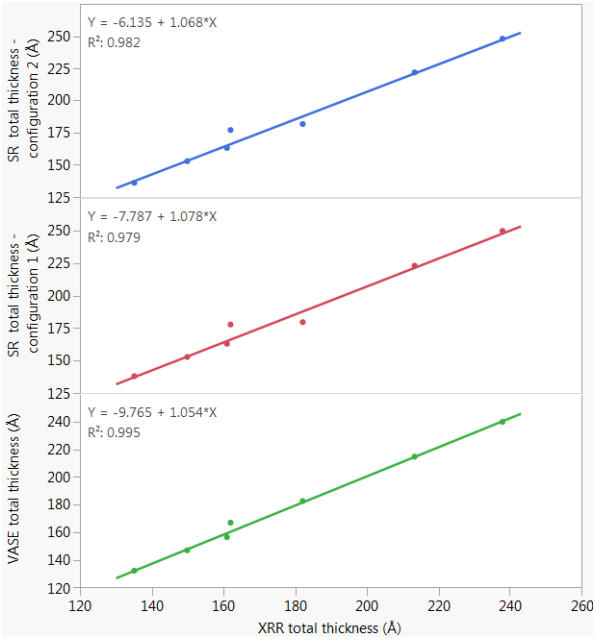

Figure 8 XRR total TiN thickness vs VASE and SR data for two configurations.

3.4 Additional model metrics based on TiN alloy coefficient

We have seen that the optical properties of metal change with thickness. In addition we are able verify if the alloy model parameter corresponds to the nominal TiN thickness. The thickness value of TiN can analytically be calculated by using the alloy coefficient. To get this alloy fraction as result it needs to be a floating parameter in the model. First we use the alloy coefficient that is result of interpolation of the set of nk curves of TiN alloy model as shown in Figure 7. Next we normalize the alloy coefficient to the nominal TiN thickness range. We analytically calculate the thickness from the alloy coefficient. Such calculated thickness we call fictitious TiN thickness (Ft). For instance, if the alloy coefficient is 0.5 and the maximal TiN thickness described by the alloy n&k's set is 345 Å, the Ft would be the product of the alloy coefficient (0.5) and the maximal thickness (345 Å) resulting in an Ft of 172,5 Å. We illustrated the usage of this fictitious TiN thickness in Figure 9. We build the alloy model from the *n&k*'s set shown in Figure 6. The TiN thickness range of 25 Å - 140 Å is too small to describe all TiN nominal thicknesses of TiN wafer set. The measured stack consists of the TiN and dielectric layers as shown in Figure 2. Our alloy model more closely describes wafer with thinner TiN layer and therefore the confidence level is good (green points). With thicker TiN layer, the stack moves further and further from the working limits of the alloy model. This is why the confidence level of correlation between - obtained TiN thickness and fictitious TiN thickness (thickness calculated based on the alloy parameter) gets worse. In ideal case the obtained thickness should correspond to the thickness calculated from the alloy coefficient. In all cases goodness of fit was good for all wafers. Therefore, quality of the metal model should be also judged based on the proposed approach. The presented data do not include the roughness layer.

Downloaded From: http://proceedings.spiedigitallibrary.org/ on 04/30/2017 Terms of Use: http://spiedigitallibrary.org/ss/termsofuse.aspx

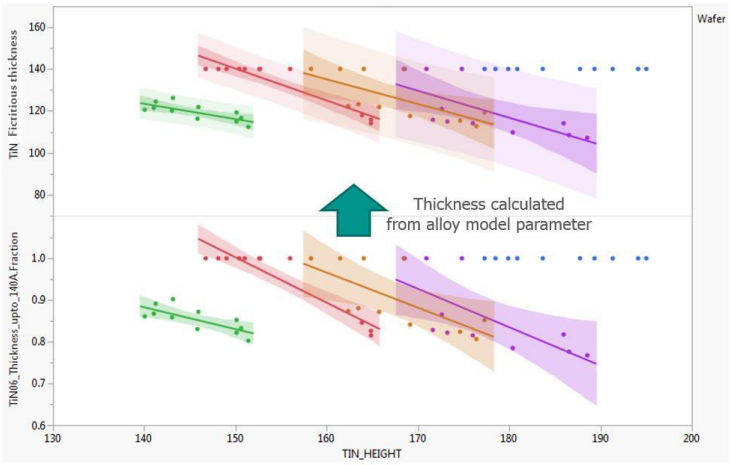

Figure 9: Graph shows alternative metrics for optical model confidence estimation that provide additional information on model correctness.

Other application of fictitious thickness approach is presented on Figure 10. We compare the same model using the data from the two SR configurations. The total TiN thickness data corresponds to Figure 8. As one can see, the SR configuration 2 data shows better correlation to the XRR reference. And this corresponds to better correlation between total thickness and fictitious thickness for SR configuration 1 over SR configuration 2.

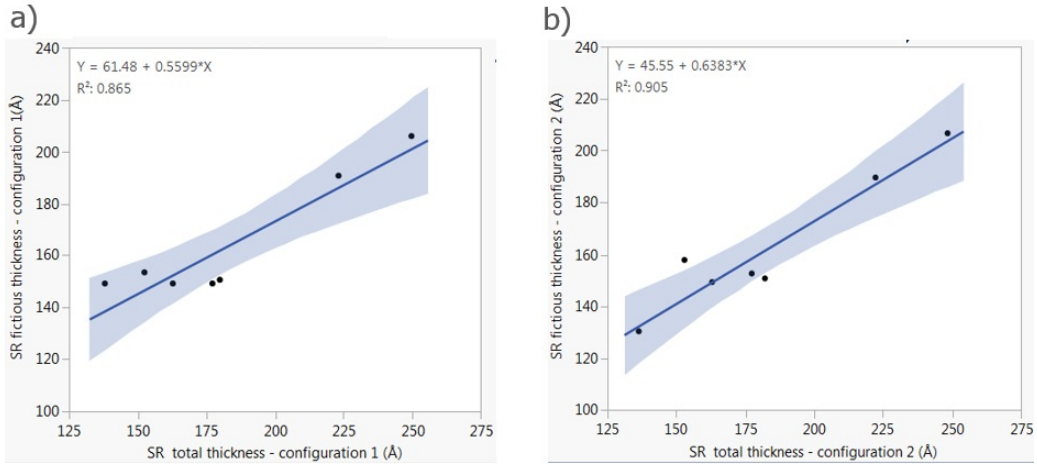

Figure 10: Correlation plot of total thickness vs fictitious thickness (calculated from alloy fraction) for two SR configurations: (a) configuration 1, (b) configuration 2.

Other application of fictitious thickness deduced from of the alloy coefficient is related to process signature tracking and model excursion as shown in Figure 11. One can see that for the first two wafers the real TiN thicknesses and its fictitious values are pretty much in agreement but for the last wafer the agreement is poor.

Downloaded From: http://proceedings.spiedigitallibrary.org/ on 04/30/2017 Terms of Use: http://spiedigitallibrary.org/ss/termsofuse.aspx

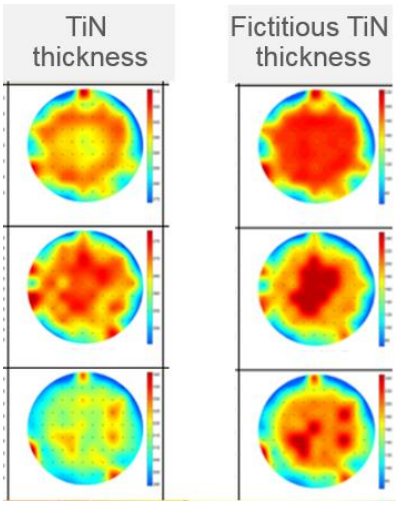

Figure 11 Wafer maps for thickness and fictitious TiN thickness from multi-layer 1D model with TiN HM.

3.5 Application of TiN alloy model in OCD modeling

Accurate determination of the TiN material properties allows one to improve the OCD solution. In this chapter we demonstrate our achieved improvement on the TiN hard mask open step. Typical structure of this step is depicted in Figure 1. The parameters of interest are: TiN recess, trench CD, and trench depth. We used as reference data a set of inline CD-SEM and AFM data. CD-SEM data were collected from column-exposure matrix (CEM) wafers. The CEM wafer setup was used to achieve a sufficient CD range. In order to achieve variability for depth, a DoE on TiN HM etch has been performed. The DoE conditions are illustrated in Figure 12. We compare four product wafers measured with full-wafer mapping. For CD results both models show a comparable data range with some offset. We can expect comparable performance for the CD parameter. However, the most important parameter is TiN recess. To evaluate model performance on recess the parameter the TiN HM was etched with three different etch times: POR (process of record), OE (overetch), and UE (underetch) conditions. For the UE conditions TiN HM is not completely open. Both models indicate close to zero recess and that agrees with DoE process conditions. On the other hand, OE condition should result in recess higher than POR. And indeed, both models show higher recess than for POR. We also had one more wafer with OE for the SiON layer. This should result in slightly higher recess than POR. The latter is also reflected in both models. Thus, we can conclude that both models correctly reflect the performed etch DoE on the recess parameter for all conditions. However, OCD model utilizing the TiN alloy model shows a smaller range on recess and higher recess values. Next we compared the real TiN thickness for both models as shown in Figure 13. Additionally, we plot the fictitious thickness for the alloy model. For the POR model the TiN material properties were fixed. In the presented data set all wafers have the same values as deposited TiN thicknesses. Since TiN is covered with a top layer we do not expect significant influence of TiN or SiON etch DoE on the TiN layer thickness. Indeed, both models show comparable average thickness except one wafer presenting a larger offset between POR and the TiN alloy models. Furthermore the POR model shows a higher TiN thickness range than the TiN alloy model. The higher range of the POR model might be due to the TiN material variability across the wafer. One of the measures of the variability can be the fictitious thickness. As described in previous section (3.4), the fictitious thickness is an analytically calculated thickness from an alloy parameter that is floated in our model. The alloy parameter describes the composition variation of the TiN material. However, if we compare fictitious thickness with nominal TiN thickness values, the fictitious thickness range is higher. Interestingly, the average value of the fictitious thickness is close to the nominal thickness of TiN. This indicates that the alloy model represents TiN in an appropriate manner. The higher range of fictitious thickness values might be a result of overfitting on other material properties/dimensions of 2D model. There is also a difference in fictitious thickness parameter between 1D and 2D solutions. Correlation between fictitious thickness and modeled TiN thickness is lower for 2D solutions. As previously mentioned, one of the reason could be data overfitting since the 2D model has more floating parameters. Another reason might be slightly different properties of TiN in the grating structure as a result of processing. The TiN interface and oxidation were discussed in more details in chapter 3.3.

Downloaded From: http://proceedings.spiedigitallibrary.org/ on 04/30/2017 Terms of Use: http://spiedigitallibrary.org/ss/termsofuse.aspx

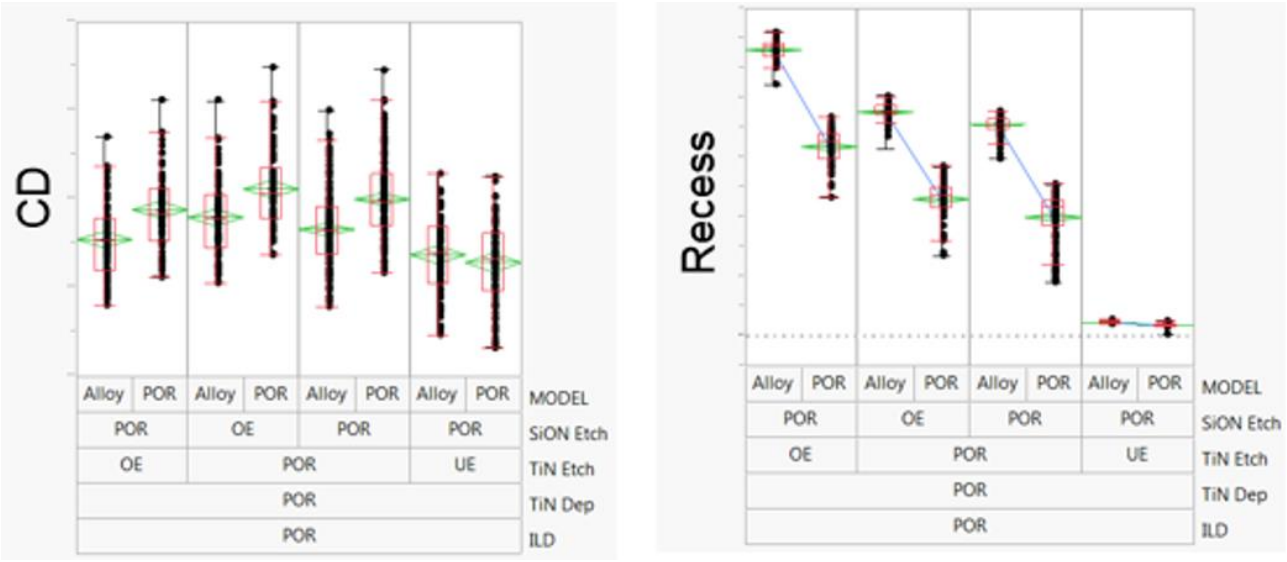

Figure 12 POR and TiN alloy model comparison on four wafer DoE set. Left graph represents comparison for middle CD values. Right graph represents comparison for recess parameter.

To evaluate the performance of the POR and TiN alloy models we correlate the DoE data to CD-SEM and AFM. Figure 14 shows TMU and linear correlation results for CEM wafer. Both POR and TiN alloy models shows similar performance for CD-SEM data matching. The POR model shows slightly better results since the TMU value is a little lower than for the TiN alloy model and R^2 is a bit higher. On the other hand, slope of linear regression in case of the TiN alloy model is equal to one, - faintly better than for the POR model. The situation is very different if we compare trench depth data with AFM as shown in Figure 15. In this case the OCD model utilizing the TiN alloy modeling approach shows much better matching to the reference. This fact illustrates that accurate TiN modeling improves the OCD model precision significantly. One of the advantages is compensation for the TiN material variability; other is that additional material information can be extracted from the analysis. The alloy model of variable thicknesses enables quick OCD model tuning and therefore shortens time to solution during the development process.

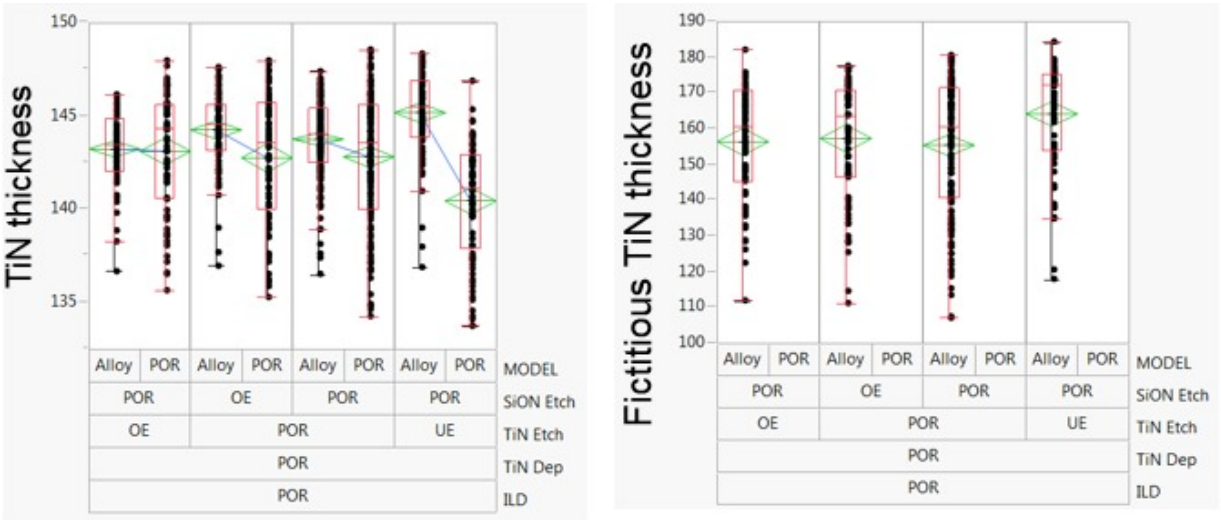

Figure 13. POR and TiN alloy model comparison on four wafer DoE set. Left graph represent comparison for TiN thickness values. Right graph represents fictitious TiN thickness obtained for OCD model using the TiN alloy approach.

Downloaded From: http://proceedings.spiedigitallibrary.org/ on 04/30/2017 Terms of Use: http://spiedigitallibrary.org/ss/termsofuse.aspx

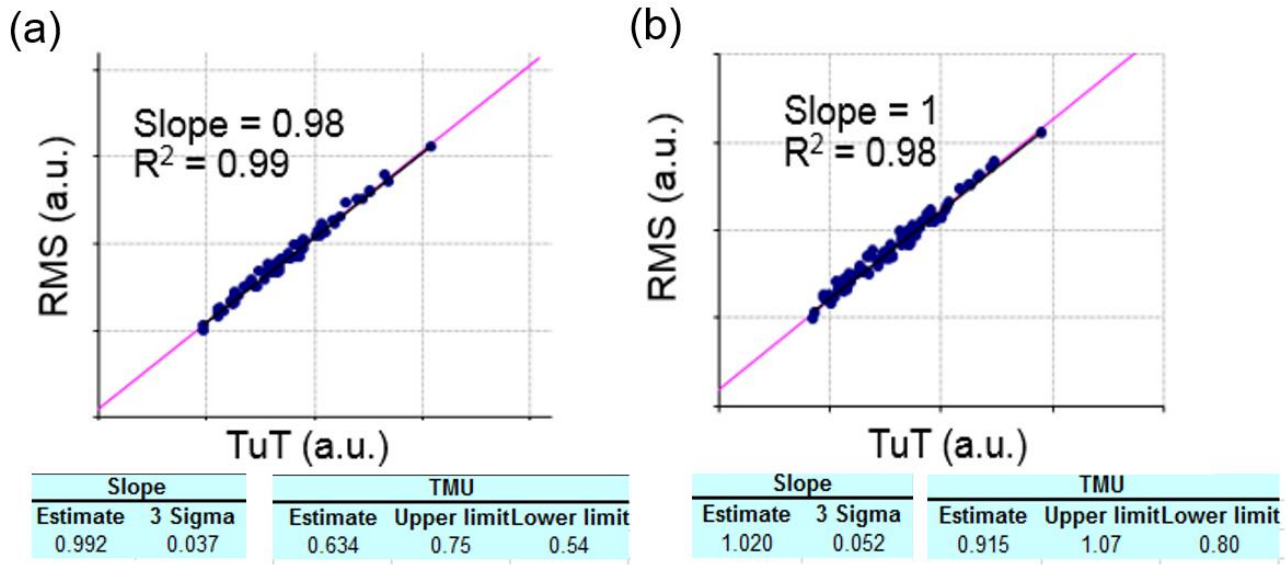

Slope		TMU		
Estimate	3 Sigma	Estimate	Upper limit	Lower limit
0.992	0.037	0.634	0.75	0.54

Slope		TMU		
Estimate	3 Sigma	Estimate	Upper limit	Lower limit
1.020	0.052	0.915	1.07	0.80

Figure 14 TMU (total measurement uncertainty) results for CD-SEM and OCD models from CEM wafer: a) the results for POR model; b) the results for TiN alloy model.

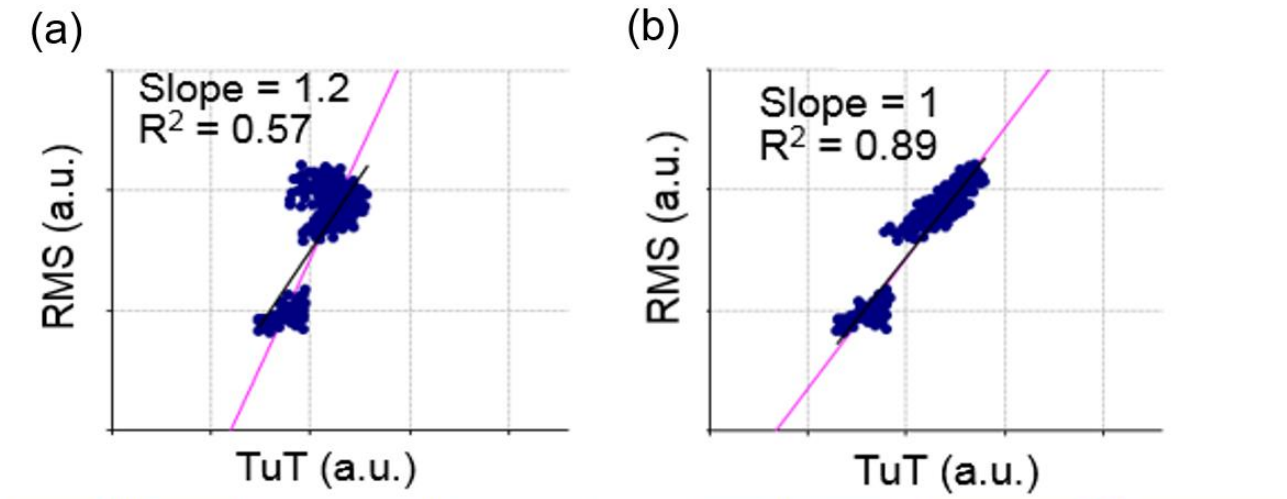

Slope		TMU		
Estimate	3 Sigma	Estimate	Upper limit	Lower limit
1.791	0.233	4.299	4.67	3.97

Slope		TMU		
Estimate	3 Sigma	Estimate	Upper limit	Lower limit
1.083	0.060	0.446	0.90	0.00

Figure 15 Correlation and TMU (total measurement uncertainty) for CD-SEM and OCD models on CEM wafer: a) the results for POR model; b) the results for TiN alloy model.

Downloaded From: http://proceedings.spiedigitallibrary.org/ on 04/30/2017 Terms of Use: http://spiedigitallibrary.org/ss/termsofuse.aspx

CONCLUSIONS

We discussed advanced optical modeling of the TiN metal hardmask for scatterometry applications. We demonstrated that TiN metal thickness dependence on dielectric function can be accounted using alloy model. Precision of OCD model can be improved by applying alloy model that assumes TiN thickness dependence via floating alloy parameter. Furthermore, we report thickness dependence on dielectric function of TiN metal used as hardmask material up to 345 Å. The thickness dependence starts to have smaller effect on the TiN optical properties for thicknesses range above 250 Å. Typically, the literary data report the thickness dependence of optical properties for thin metal films up to 100 Å-thick. Finally, we demonstrated that the alloy coefficient normalized to nominal thickness of the developed TiN alloy model provides an additional information regarding model accuracy. Our findings are applicable to lower technology nodes where the TiN films are also widely utilized. Proposed modeling methodology is relevant for TiN metal used in transistor gate stack and barrier and applicable to other thin metals as well.

ACKNOWLEDGMENTS

The research leading to these results has received funding from the ENIAC Joint Undertaking under grant agreement No.621280 “E450LMDAP”.

The authors wish to acknowledge Mr. Steffen Brunner (GLOBALFOUNDRIES, Germany) who performed some initial measurements used to formulate optical model

REFERENCES

[1] M. S. R. N. Kiran, M. G. Krishna, and K. A. Padmanabhan, "Growth, surface morphology, optical properties and electrical resistivity of ε-TiNx (0.4 < x ≤ 0.5) films," *Applied Surface Science* **255**(5, Part 1), 1934-1941 (2008).
[2] L. Liechao, J. Kang, and J. Wen, "Low Stress TiN as Metal Hard Mask for Advance Cu-Interconnect," *ECS Transactions* **44**(1), 481-486 (2012).
[3] X. Zhigang et al., "PVD TiN hardmask for copper metallization," *Semiconductor Manufacturing, 2007. ISSM 2007. International Symposium on* 1-3 (2007).
[4] H. Fujiwara, Ed., *Spectroscopic Ellipsometry: Principles and Applications*, John Wiley & Sons Ltd, (2007).
[5] G. K. Pribil, B. Johs, and N. J. Ianno, "Dielectric function of thin metal films by combined in situ transmission ellipsometry and intensity measurements," *Thin Solid Films* **455–456**(0), 443-449 (2004).
[6] C. Liu et al., "Thickness determination of metal thin films with spectroscopic ellipsometry for x-ray mirror and multilayer applications," *Journal of Vacuum Science & Technology A: Vacuum, Surfaces, and Films* **17**(5), 2741-2748 (1999).
[7] J.N. Hilfiker, N. Singh, T. Tiwald, D. Convey, S.M. Smith, J.H. Baker, H.G. Tompkins, “Survey of methods to characterize thin absorbing films with spectroscopic ellipsometry”, *Thin Solid Films* 516, 7979-7989 (2008).
[8] P. B. Barna, and M. Adamik, “Fundamental structure forming phenomena of polycrystalline films and the structure zone models,” Thin Solid Films, 317(1–2), 27-33 (1998).
[9] M. Hövel, B. Gompf, and M. Dressel, "Dielectric properties of ultrathin metal films around the percolation threshold," *Physical Review B* **81**(3), 035402 (2010).
[10] Y. Yagil, and G. Deutscher, "Scaling and renormalization in transmittance of thin metal films near the percolation threshold," *Applied Physics Letters* **52**(5), 373-374 (1988).
[11] N. Posseme, T. Chevolleau, R. Bouyssou et al., “Residue growth on metallic-hard mask after dielectric etching in fluorocarbon-based plasmas. I. Mechanisms,” Journal of Vacuum Science & Technology B, Nanotechnology and Microelectronics: Materials, Processing, Measurement, and Phenomena, 28(4), 809-816 (2010).
[12] M. Darnon et al., "Undulation of sub-100nm porous dielectric structures: A mechanical analysis," *Applied Physics Letters* **91**(19), 194103 (2007).
[13] E. Kaulfersch et al., "Finite element analysis for BEOL stress engineering to improve yield and reliability of sub-30 nm structures," *Semiconductor Conference Dresden-Grenoble (ISCDG), 2013 International* 1-4 (2013).

Downloaded From: http://proceedings.spiedigitallibrary.org/ on 04/30/2017 Terms of Use: http://spiedigitallibrary.org/ss/termsofuse.aspx

[14]J. Ducoté et al., "Prediction of porous dielectric line wiggling phenomenon with metallic hard mask: From simulation to experiment," *Applied Physics Letters* **104**(23), 231603 (2014).

Downloaded From: http://proceedings.spiedigitallibrary.org/ on 04/30/2017 Terms of Use: http://spiedigitallibrary.org/ss/termsofuse.aspx